







Original Article

## Trigger mechanism of loess-mudstone landslides inferred from ring shear tests and numerical simulation

WANG Xin-gang  <https://orcid.org/0000-0002-1744-8712>; e-mail: xgwang@nwu.edu.cn

LIAN Bao-qin\*  <https://orcid.org/0000-0002-3419-5040>;  e-mail: qin20054184@126.com

Liu Kai\*  <https://orcid.org/0000-0002-4038-653X>;  e-mail: liukaii@stumail.nwu.edu.cn

Luo Li  <https://orcid.org/0000-0002-8603-9234>; e-mail: 1577062495@qq.com

\*Corresponding author

State Key Laboratory of Continental Dynamics, Department of Geology, Northwest University, Xi'an 710069, China

**Citation:** Wang XG, Lian BQ, Liu K, et al. (2021) Trigger mechanism of loess-mudstone landslides inferred from ring shear tests and numerical simulation. *Journal of Mountain Science* 18(9). <https://doi.org/10.1007/s11629-021-6791-6>

© Science Press, Institute of Mountain Hazards and Environment, CAS and Springer-Verlag GmbH Germany, part of Springer Nature 2021

**Abstract:** Whereas loess-mudstone landslides are widely distributed and frequently occurred at the loess Plateau, this type of landslides is hard to detect due to its particularity, and easily generates serious losses. To clarify the shear characteristics and formation mechanism of loess-mudstone landslides, field investigations, ring shear tests and numerical simulation analyses were performed on the loess specimens collected from the Dingjiagou landslide in Yan'an city, China. The test results showed that both the peak strength and residual strength of slip zone soils have a decreasing tendency with moisture content, while the increasing of normal stress caused an increase in the shear strength. These phenomena indicate that the rise in the moisture content induced by precipitation or the decreasing of normal stress due to excavation activities would result in the weakening of slip zone soils. Numerical simulations of the evolution process of slope failure using the finite element method were conducted based on the Mohr–Coulomb criterion. It was found that the heavy precipitation played a more important role in the slope instability compared with the excavation. In addition, the field investigation showed that loess soils with well-developed cracks and underlying

mudstone soils provide material base for the formation of loess-mudstone landslides. Finally, the formation mechanism of this type of landslides was divided into three stages, namely, the local deformation stage, the penetration stage, the creeping - sliding stage. This study may provide a basis for understanding the sliding process of loess-mudstone landslides, as well as guidelines for the prevention and mitigation of loess-mudstone landslides.

**Keywords:** Loess-mudstone landslides; Slip zone soil; Ring shear tests; Numerical simulation; Formation mechanism

### 1 Introduction

Loess-mudstone landslides are one of the most catastrophic slope instability phenomena that has distributed widely and occurred frequently in the Loess plateau (Wen et al. 2005; Wen and He 2012), posing a serious risk to construction infrastructures and human lives. Thus, there has been many researchers paid attention to the mechanical behavior of loess-mudstone landslides soils (Kimura et al. 2015; Mu et al. 2019; Peng et al. 2015; Peng et al. 2016).

**Received:** 17-Mar-2021

**Revised:** 01-Jun-2021

**Accepted:** 28-Jun-2021

Loess-mudstone landslides are referred to as one type of landslides that slides along a contact surface between loess soils and its underlying Neogene-age mudstones (Wen and He 2012). This type of landslides generally occurs on very flat terrain with a short run-out distance. Under the subsequent influence of the geological activities and human activities that caused the sliding cracks to be covered, the shape characteristics of landslides is not obvious and is hard to be detected (Wu et al. 2014a). However, foundations for buildings are often installed on such unstable landslide slopes as the construction lands available become more and more scarce, causing catastrophic hazards upon precipitation (Juang et al. 2019). Therefore, to construct foundations on loess-mudstone landslides more stable and safer, it is necessary to understand the triggering factors and failure mechanism of this type of landslides.

To date, there have been considerable researches for understanding the properties of loess-mudstone landslides (Peng et al. 2015; Wen and He 2012; Wu et al. 2014b; Zhang et al. 2017). For instance, many authors have examined the deformation properties of loess-mudstone landslides (Wen and He 2012; Wu et al. 2014a). Chen et al. (2014) pointed out that the slip zone soils of loess-mudstone landslides exhibit strain-softening behavior, which may be caused by the existing of fine soil particles such as expanded clay particles in the slip zone soils. Peng et al. (2016) conducted a field survey on the Liujiabu loess-mudstone landslide and concluded that the evolution process of landslides is controlled by the fault fracture. Li et al. (2016) carried out a semi-similar material physical model test to investigate the initiating conditions of precipitation-induced loess-mudstone landslides and proposed that the initiation of landslides are related to factors such as precipitation intensity, duration and thickness of overlying loess soils. More recently, Wang et al. (2019) reported that water would gradually accumulate above a relatively impermeable layer (i.e., the Tertiary mudstone), causing the soil above to be softened and triggering landslides eventually.

Shear strength parameters including the peak strength and residual strength of slip zone soils play significant roles for assessing the slope stability (Lian et al. 2020). The composition of slip zone soils obtained from loess-mudstone landslides is very complex and will be changed over time, the understanding of the mechanical properties for slip

zone soils is therefore important for clarifying the formation mechanism of loess-mudstone landslides (Wen and He 2012). For instance, it has been found that using a direct shear test, the kinematic history of the slip zone can be reconstructed (Wen and Aydin 2003). Furthermore, the shear behavior of slip zone soils obtained from a loess-mudstone landslide was investigated by using a triaxial compression test and the results showed that the fully soften shear strength of soils at the low normal stress level is greater than that at the high normal stress level (Kimura et al. 2015). More recently, Mu et al. (2019) proposed the correlation between the moisture content and the shear strength of slip zone soils, and pointed out that the increase in the moisture content of a loess-mudstone interface causes a reduction in the shear strength of slip zone soils. By now, the residual strength has been mainly determined by using the reversal direct shear test and ring shear tests (Sassa et al. 2004; Wang et al. 2014), while the triaxial compression test is not preferred (Vithana et al. 2012). By adopting a ring shear apparatus, the soil samples could be sheared at a surface with a constant area at large shear displacements, which could better simulate landslides in the field site (Garga et al. 1971; Lian et al. 2019). Up to now, some researchers have made attempts to investigate the formation mechanism of loess-mudstone landslides (Mu et al. 2019; Wu et al. 2014b). However, the formation mechanism of loess-mudstone landslides is very complicated and may differ from one another in fundamental ways. Therefore, the formation mechanism of this type of landslides requires more experimental evidence as well.

The main goal of present work is to clarify the triggering factors and failure mechanism of loess-mudstone landslides through ring shear tests and numerical analysis of a slope under various conditions, taking into account the field condition at the site in the study area.

## 2 Background of the Study Site

The landslide occurred at 36°38′38.62″N, 109°32′15.24″E, in the Dingjiagou village (hereinafter referred to as the DJG landslide) in Yan'an city (Fig. 1a), China, on 4th June, 2016, with a volume of approximately  $105 \times 10^4 \text{ m}^3$  (350 m wide from the south to the north, 180 m long from the east to the

west and 20 m thick in average). The main slide movement was eastern-dip, and the elevation in the northwest was higher compared with that in the southeast, with the height difference of about 70 m. The dip direction was in a range of 75-85°. Due to the excavation activities (Fig. 1b) at the front edge of an ancient landslide during a foundation construction of a building, the ancient landslide was reactivated and a special double sliding surfaces was induced consequently (Fig. 1c). It was found that the landslide debris was mainly composed of loess soils with mudstones bedrocks and then was classified as a typical loess-mudstone landslide (Fig. 1d). In addition, the slip zone soils, varied in thickness (with about 30 cm in average), were a mixture of the upper loess soils and the lower part of the strongly weathered

Neogene-age mudstones. The shearing surface at the front part was found relatively smooth (Fig. 1f), in which the soil particles showed an obvious orientation and evident scratches (Fig. 1g). The slip zone soils were collected at the sampling site and then taken back to the laboratory to conduct tests.

The magnitude of the average monthly precipitation in the study area varied over time (Fig. 2). It is clear that the wet months in the study area tended to be in July and August. In the periods of consideration (in last 20 years), the greatest measured precipitation was roughly 120 mm, while the lowest level of precipitation was close to 0 mm at the start and the end of the year (Fig. 2). Interestingly, the number of geological hazards such as landslides and collapse changed over time, and most of the

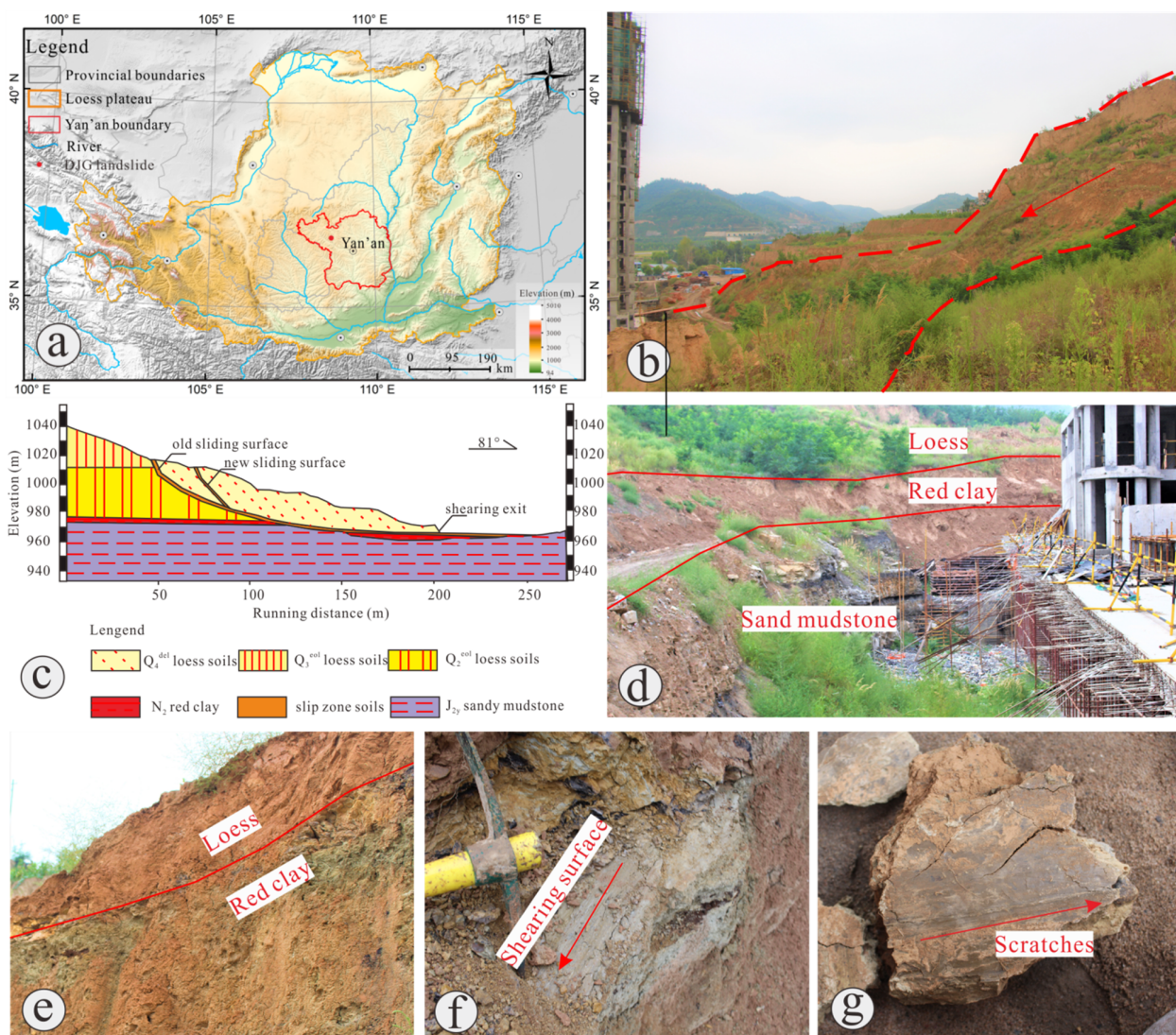


**Fig. 1** Study area. (a) Location of the study area; (b) The overview from the toe part of the landslide; (c) Longitudinal section along the main sliding path; (d) Excavation at the toe of the slope; (e) Sampling site; (f) Shearing surface; (g) Scratches.

geological hazards occurred in the wet months (from June to August). Clearly, the frequent occurrence of the landslides is closely associated with the magnitude of precipitation. Therefore, the ring shear tests were conducted on specimens with different moisture contents to clarify the formation mechanism of loess-mudstone landslides associated with precipitation.

### 3 Materials and Methods

#### 3.1 Testing sample

The soil samples were collected from the back scarp of the DJG landslide (Fig. 1e). Two soils samples (S1 and S2) were used to determine Grain size distribution of the specimens by using a laser particle size analyzer Battersize 2000 (Dandong Battersize Instruments Corporation, Dandong, China). The grain size distribution was illustrated in Fig. 3. The results of S1 showed that the soil sample contains about 24.5% of clay (<0.002 mm), 74.5% of silt soils (0.002-0.075 mm), and 1% of sand (0.075-0.05 mm). Following the *Annual Book of ASTM Standards* (ASTM 2006), some basic properties (the plastic limit, the liquid limit and the specific gravity) of samples were determined and summarized in Table 1. The results showed that the average value of plastic limit, liquid limit and specific gravity of the specimens are 21.5, 37.7, and 2.67, respectively. By using the oven-drying method, it is found that the initial bulk density and natural water content of the slip zone soils are 2.09 g/cm<sup>3</sup> and 19.65%, respectively.

#### 3.2 Testing procedure

As mentioned above, the normal stress and moisture content have a significant influence on the shear behavior of loess-mudstone landslides (Li et al. 2016; Wen et al. 2005). To clarify the effect of normal stress and moisture content on the loess-mudstone landslides, ring shear tests were conducted on soil samples with different initial normal stresses and moisture contents.

**Table 1** Physical properties of the soil samples

Sample No.	$W_n$	$\rho$	$G_s$	$W_L$	$W_p$	Grain size fractions (%)		
						<0.002 mm	0.002-0.075 mm	0.075-0.05 mm
S1	19.8	2.1	2.67	38	21.5	24.5	74.5	1
S2	19.5	2.08	2.66	36	21	26	73.2	0.8

**Notes:**  $\rho$ = Bulk density (g/cm<sup>3</sup>);  $G_s$ =Relative density;  $W_n$ = Natural water content (%);  $W_L$ = Liquid limit (%);  $W_p$ = Plastic limit (%).

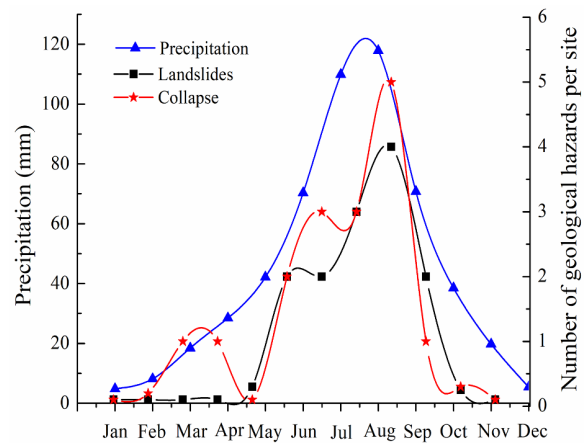


**Fig. 2** Average monthly precipitation and geological hazards in the study area in last 20 years.

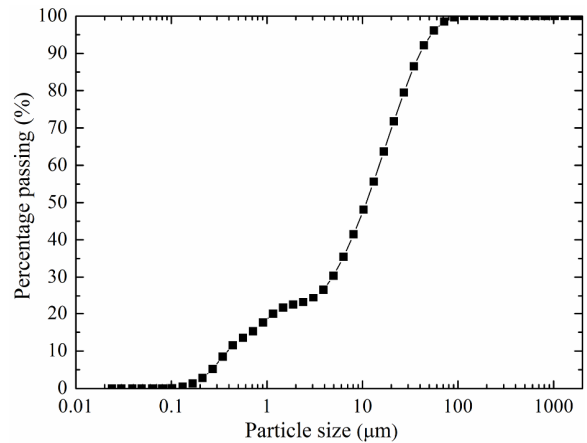


**Fig. 3** Soil grain distribution of slip zone soils (S1).

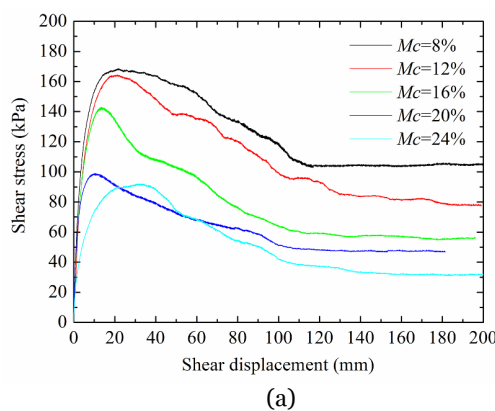
The testing procedure includes three basic steps. The first step is sample preparation. The soil sample was placed in an oven at about 105°C for about 48 h to remove the moisture content completely. Then, the soil sample was crushed and oven-dried and passed through a 2.0 mm sieve. After that, about 2000 g of dried soils were weighed by using a weighting scale, and then a specific distilled water was added to the soils to achieve the target water contents (8%, 12%, 16%, 20% and 24%). Finally, the remolded soil samples, which have been prepared, were kept in a sealed container for about 24 h to achieve a uniform distribution of water. The second step is sample installation. The soil sample was poured into the

shear box of the SRS-150 ring shear apparatus developed by GCTS Company for consolidation. The SRS-150 ring shear apparatus, which is manufactured by GCTS Company, is used in current study. The ring shear specimen is annular with an inside diameter of 100 mm, an outside diameter of 150 mm and a height of 25 mm. The apparatus allows for the application of axial loads up to 10 kN, normal stress up to 1000 kPa, and shear stress up to 1300 kPa. In this phase, the soil sample was placed in three layers in the shear box to achieve a uniform sample while packing. The interface between the adjacent layers was scarified to obtain a more uniform soil sample. The third step is sample consolidation and shearing. After the soil sample was placed in the shear box, the soil sample was normally-consolidated with different normal stresses (100 kPa, 200 kPa, 300 kPa and 400 kPa), and then was sheared at the same normal stress level as consolidated stress until the residual strength was attained. In current study, the consolidation process was considered completely when the axial settlement rate was smaller than 0.01 mm/min according to the conclusion reported by (Yuan et al. 2019). To insure a drained condition and avoid the shear rate effect, a shear rate of 0.1 mm/min was adopted in all tests, following Wang (2014) who pointed out that the shear rate below 5 mm/min has little effect on the shear strength of loess soils.

## 4 Results

### 4.1 Shear behavior of slip zone soils under different moisture contents

To exemplify the shear behavior of slip zone soils,



five soil samples with different moisture contents (8%, 12%, 16%, 20% and 24%) were tested and their results are shown in Fig. 4. Fig. 4a plots the shear stress against the shear displacement, and Fig. 4b depicts the relationship between the shear strength (the peak strength and residual strength) and moisture content. It can be seen that in all tested samples, the slip zone soils exhibited strain-softening behavior, i.e., after the shear resistance reaches the peak value, with further increase in the shear displacement results in a reduction in the shear strength. Furthermore, it is observed that both the peak strength and residual strength showed a decreasing tendency with moisture content. To be more specific, an increase in moisture content (from 8% to 24%) of soil specimen causes a considerable reduction in peak strength (from 168.45kPa to 91.5 kPa). Comparatively, the residual strength of soil specimen tends to decrease from 104.77 kPa to 46.2 kPa when moisture content increases from 8% to 24%, decreasing about 55.9% (Fig. 4a). Fig. 4b illustrates the correlations between the shear strength and moisture content. It can be observed that both the peak strength and the residual strength show almost a linear decreasing tendency with the moisture content in a range of between 8% and 24%.

It has been found that the reorientation of soil particles along the shearing surface varies under various moisture contents (Skempton 1985; Yin et al. 2017). Similarly, we found that with a low moisture content, the soil particles on the shearing surface are arranged randomly with large edges (Fig. 5a), and the rolled steps were observed clearly at the local view of the shearing surface (Fig. 5b). As moisture content increases, the steps on the shearing surface decreases

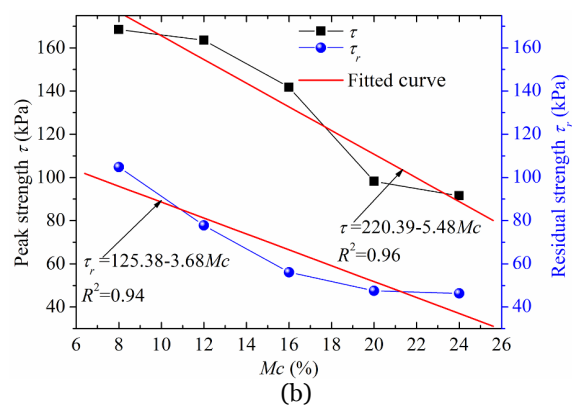


**Fig. 4** Ring shear test results on slip zone soil specimen at various moisture contents ( $\sigma_n = 100$  kPa,  $v = 0.1$  mm/min). (a) Shear stress against the shear displacement; (b) Relationship between shear strength and moisture content ( $M_c$  is moisture content).

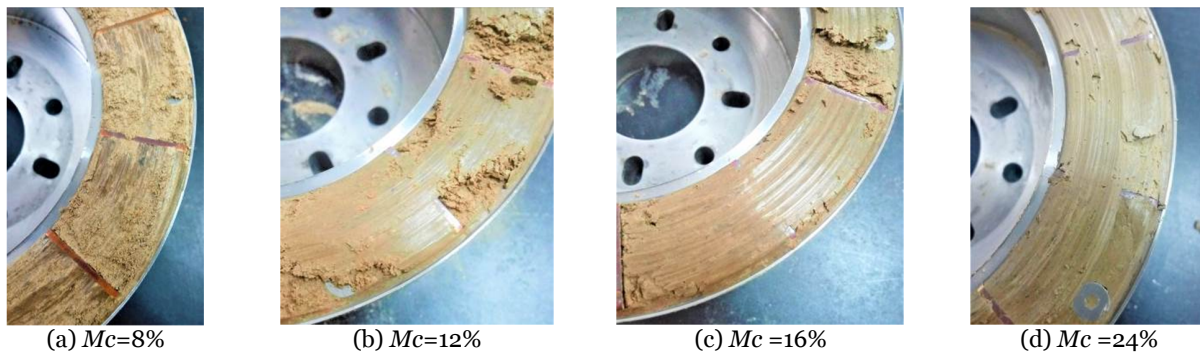


**Fig. 5** Macro morphology of shearing band at different moisture contents.

(Fig. 5c) and becomes more smooth (Fig. 5c-d). This phenomenon may be attributed to the liquefaction caused by the accumulation of fine soil particles and water on the shearing surface induced by the built up of high pore water pressure (Wang et al. 2014).

#### 4.2 Shear behavior of slip zone soils under different normal stresses

It has been long recognized that the shear behavior of soils is closely related with normal stress (Gibo et al. 1987; Motoyuki et al. 2000; Xu et al. 2018). The results of four tested samples are selected to illustrate the effect of normal stress on the shear behavior of loess-mudstone soils. Fig. 6a shows the shear stress against shear displacement. The test results revealed that an increase in the normal stress (from 100 kPa to 400 kPa) resulted in a great increase in the peak strength (from 55.28 kPa to 85.16 kPa). Furthermore, the residual strength of the specimen increased about 90%, from 43.25 kPa at the normal stress of 100 kPa to 82.65 kPa at the normal stress of 400 kPa. To quantitatively describe the correlation between shear strength and normal stress, the experimental data were fitted in Fig. 6b. It can be found that both the peak strength and the residual strength have a linear relationship with normal stress. The experimental results herein (Fig. 6) indicated that the decreasing of the normal stress would result in a reduction in shear strength, leading to shear failures and eventually triggering the occurrence of landslides.

The residual strength is an important parameter for evaluating the stability of slopes (Gibo et al. 2002). In order to compare the normal stress effect on the shear behavior of slip zone soils, the stress ratio which is defined as the shear stress divided by the normal stress is proposed following (Eid et al. 2016). The typical stress ratio is plotted in Fig. 6c against the

corresponding normal stress. It can be seen from that the magnitude of the stress ratio at lower normal stress levels is higher than that at higher normal stress levels. This finding is consistent with the results reported in the literature (Maksimovic, 1989; Tiwari and Marui 2005). The nonlinearity of the stress ratio-normal stress curve is more pronounced at lower normal stress levels, indicating that selecting an appropriate normal stress range to determine the residual strength of slip zone soils obtained from a shallow slope with a low overburden pressure is essential for accurately assessing the stability of a slope.

## 5 Numerical simulation of the evolution process of slope failure

There has been many researchers using finite element techniques to investigate the landslide hazards (Cremonesi et al. 2011; Mulligan et al. 2020; Zhu and Randolph 2010). As the implementation of the numerical simulation make possible to observe the changes of quantitative characteristics such as stress distribution and deformation properties that may be difficult to observe in the physical model testing, thus, the evolution process of a slope failure was simulated under different conditions (i.e., self-weight, heavy precipitation and excavation) by using the finite element method and GeoStudio 2007 computer software in current work, and the stress distribution, as well as the deformation characteristics of the slope was presented in the following sections.

### 5.1 Model description

It is widely acknowledged that precipitation and excavation activities have a great influence on the

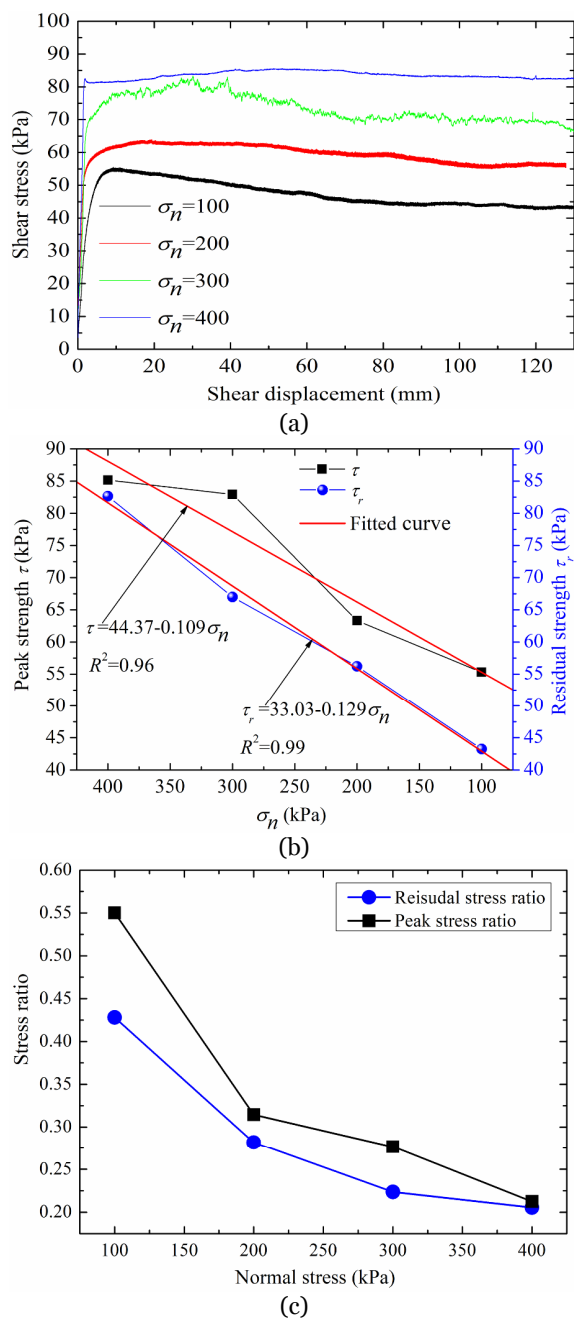


**Fig. 6** Ring shear test results on slip zone soil specimen under various normal stresses ( $M_c = 28\%$ ,  $v = 0.1 \text{ mm / min}$ ): (a) Shear stress against the shear displacements; (b) Relationship between shear strength and normal stress; (c) Stress ratio against normal stress.

stability of a slope (Mu et al. 2019; Peng et al. 2019). Therefore, numerical analysis with four engineering cases (Case I: a natural slope; Case II: a natural slope subjected to precipitation; Case III: a natural slope subjected to excavation; Case IV: a natural slope subjected to excavation and then precipitation) was

performed to successively elucidate the mechanism of slope failure in a series.

The numerical modeling of the slope, with a height of 103 m on the left, a height of 33 m on the right, and a length of 270 m at the bottom, was established according to the main sliding section of the landslide (Fig. 1d). As shown in Fig. 7, the predominantly dark green, dark brown, gray and yellow areas show  $Q_3$  loess soils,  $Q_2$  loess, mudstone and the excavated  $Q_4$  loess soils, respectively. In addition, the orange banded mesh and the bright blue banded mesh represent the red clay and the old sliding surface (slip zone soils in Table 2), respectively. All geometric dimensioning of stratum including such as  $Q_3$  loess soils,  $Q_2$  loess, mudstone and the thickness of sliding zones were modeled according to the geological survey report. The boundary conditions of the model in this section are listed as follows: the boundaries with x-coordinates equal to 0 and 270 are fixed in the x-direction and y-direction, and the left side and the right side of the model are fixed in the x-direction.

**Table 2** Input parameters used in the numerical model

Lithologic character	Unit weight (kN/m <sup>3</sup> )	Friction angle (°)	Cohesion (kPa)	Poisson's ratio	Elastic Modulus (kPa)
$Q_4$ loess	18.5	19.2	43.5	0.23	67000
$Q_3$ loess	19.4	20.3	47.8	0.23	75000
$Q_2$ loess	22.7	21.2	53.3	0.26	87000
$N_2$ red clay	24.3	21.6	58.2	0.27	99000
Slip zone soils	20.9	7.3	30.0	0.22	18000
Mudstone	25.2	45.2	880	0.33	1500000

The mechanical parameters of the soil samples affect significantly the movement characteristics of landslides. Therefore, using appropriate input parameters in the numerical model ensures a good mechanical response of soils. A series of laboratory tests (i.e., bulk density tests (determine bulk density), uniaxial compressive tests (determine Poisson's ratio), triaxial compressive tests (determine elastic modulus, cohesion and friction angle), etc.) were conducted to select material parameters used in the numerical model (Fig. 7 and Table 2). It should be noted that the strength parameters such as the cohesion and friction angle of slip zone soils were obtained on the basis of the residual strength of the saturated slip zone soil (Fig. 4), and the average bulk density of slip zone soils (Table 1) was adopted in the numerical model and listed in Table 2. The

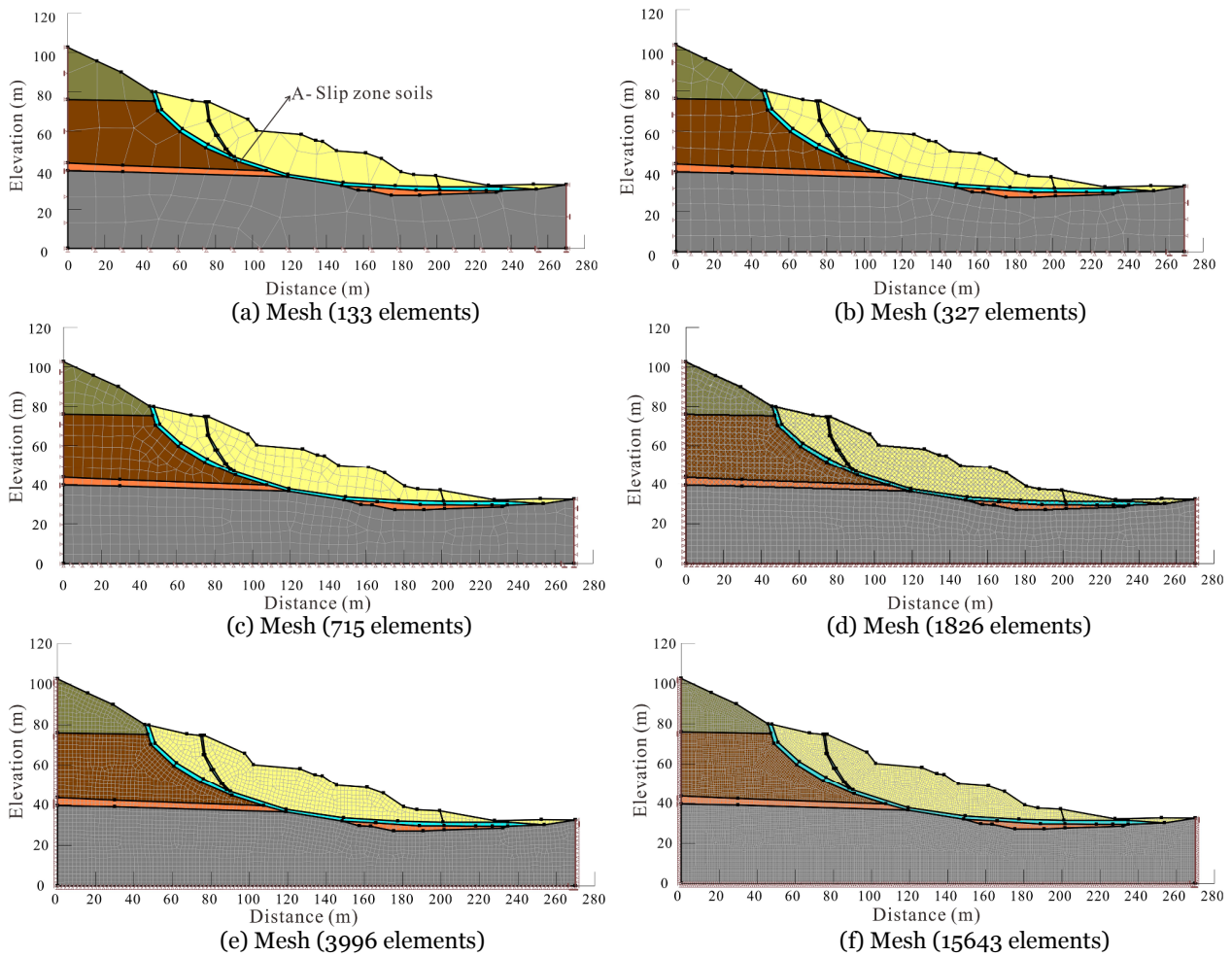


**Fig. 7** A mesh convergence study using different mesh densities. (a) Mesh (113 elements); (b) Mesh (327 elements); (c) Mesh (715 elements); (d) Mesh 1826 elements); (e) Mesh (3996 elements); (f) Mesh (15643 elements).

precipitation in intensity was set as 4 mm/day according to the data shown in Fig. 2, and the total duration of the precipitation was 30 days. The elastic-plastic constitutive model (Mu et al. 2019) was applied to the soils in current study and the soil of the slope was assumed to obey the Mohr–Coulomb failure criterion (Zhao et al. 2017).

It is widely recognized that an appropriate mesh is essential for capturing the main important characteristics of soil, which thereby producing accuracy in the obtained information (Caendish et al. 1985; Ding et al. 2007). In order to choose a suitable mesh to give an acceptable result, a mesh convergence study was performed by using six different mesh densities (Fig. 7). The number of elements used in each mesh is indicated in Fig. 7 and the results at point A for each of the six mesh densities are compared in Table 3. As listed in Table 3, an increase in the element from 715 to 15643 caused a negligible change in the maximum shear stress, the maximum

shear strain and the maximum shear displacement at point A. After performing a convergence study, an appropriate mesh configuration which has 756 nodes and 715 quadrilateral elements was determined for the site and shown in Fig. 8.

**Table 3** Results of the mesh convergence study

Numbers of elements used in each mesh	Max. shear stress (kPa)	Max. shear strain (%)	Max. shear displacement (m)
133	20	0.12	0.10
327	21	0.14	0.13
715	22	0.15	0.15
1826	22	0.15	0.15
3996	22	0.15	0.15
15643	22	0.15	0.15

**5.2 Stress, deformation and failure caused by heavy precipitation**

In slope stability analysis, the limit equilibrium method is usually adopted to calculate the factor of



safety of a slope. In current study, the Bishop method, which uses the method of slices to discretize the soil mass, was selected to determine the factor of safety of slope by using SLOPE/W software (from GeoStudio). The factor of safety of a slope is expressed as follows:

$$F_s = \frac{\sum_{i=1}^n [W_i \times \sec \alpha_i \times \tan \phi + c \times L_i] / m_i}{\sum_{i=1}^n W_i \times \sin \alpha_i} \quad (1)$$

where  $F_s$  is the factor of safety along the slip surface,  $i$  is the slice index,  $W_i$  is the weight of each slice,  $\alpha_i$  is the angle of inclination of the potential failure arc to the horizontal at the mid point of the slice,  $c$  is the effective cohesion,  $\phi$  is the effective internal friction angle,  $l$  is the width of each slice,  $m_i = (\cos \alpha_i + \tan \phi \times \sin \alpha_i / F_s)$ .

To calculate the strength characteristics of the slope, Mohr–Coulomb failure model which allows materials to harden or soften was adopted in the numerical simulation.

Calculated results are summarized in Table 4 and presented in Figs. 9-11. The shear stress contour map, the shear strain contour map and the shear displacements contour map are shown in Figs. 9-11, respectively. The factor of safety ( $F_s$ ) of a slope is determined according to the shear strength reduction technique (Erzin and Cetin 2013), and the stability state of a slope is classified based on the “code for geological investigation of landslide prevention”

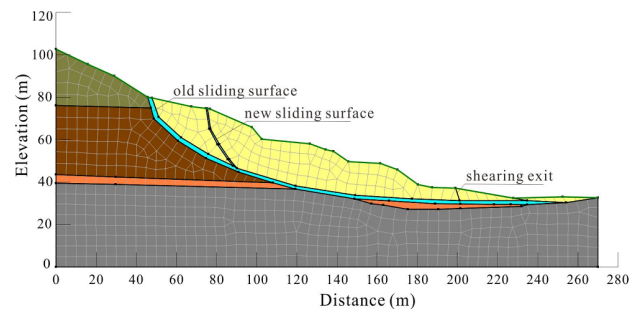


**Fig. 8** The model for a loess-mudstone slope with an appropriate mesh.

**Table 4** Calculated results by the Mohr–Coulomb failure model and stability assessment

Case	Max. s stre(kPa)	Max. s stra (%)	Max. s disp (m)	$F_s$	Stability
I	32	0.0008	0.012	1.424	Stable
II	60	0.12	0.400	1.032	Less stable
III	32	0.016	0.016	1.311	Basically stable
IV	63	0.375	1.200	0.876	Unstable

**Note:**  $F_s$ =Factor of safety. Max. s stre=Max. shear stress; Max. s stra= Max. shear strain; Max. s disp= Max. shear displacement.

(GB/T32864-2016): when the computed  $F_s$  is greater than 1.15, the slope is under stable state; when  $1.05 < F_s < 1.15$ , the slope is basically stable state; when  $1 < F_s < 1.05$ , the slope is less stable; when  $F_s$  is smaller than 1, the slope is under the unstable state.

With respect to the soils under the natural state (with only self-weight), it can be seen from Fig. 9a that, the location of the maximum shear stress is in

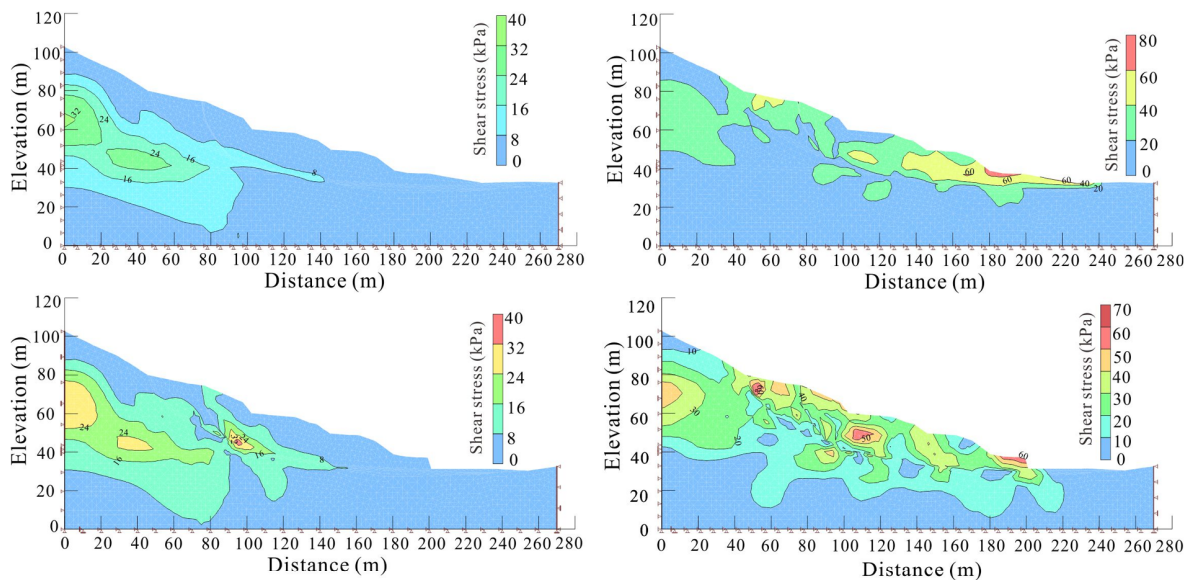


**Fig. 9** The shear stress contour map. (a) Natural slope; (b) Natural slope after heavy precipitation; (c) Natural slope after excavation; (d) Natural slope after excavation and precipitation.

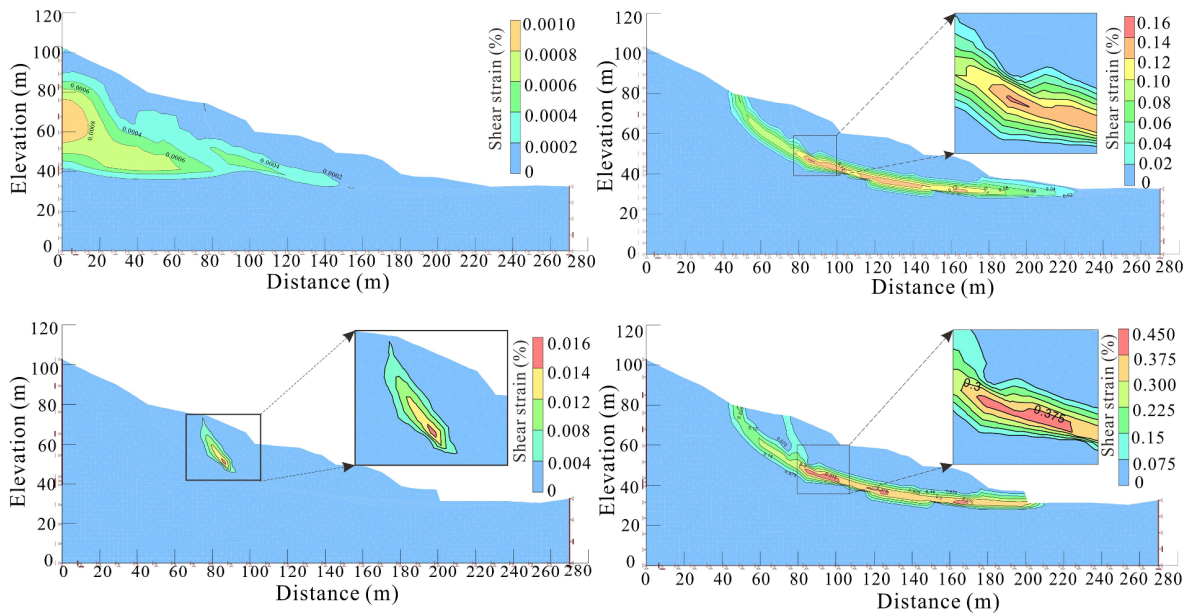


**Fig. 10** The shear strain contour map. (a) Natural slope; (b) Natural slope after heavy precipitation; (c) Natural slope after excavation; (d) Natural slope after excavation and precipitation.

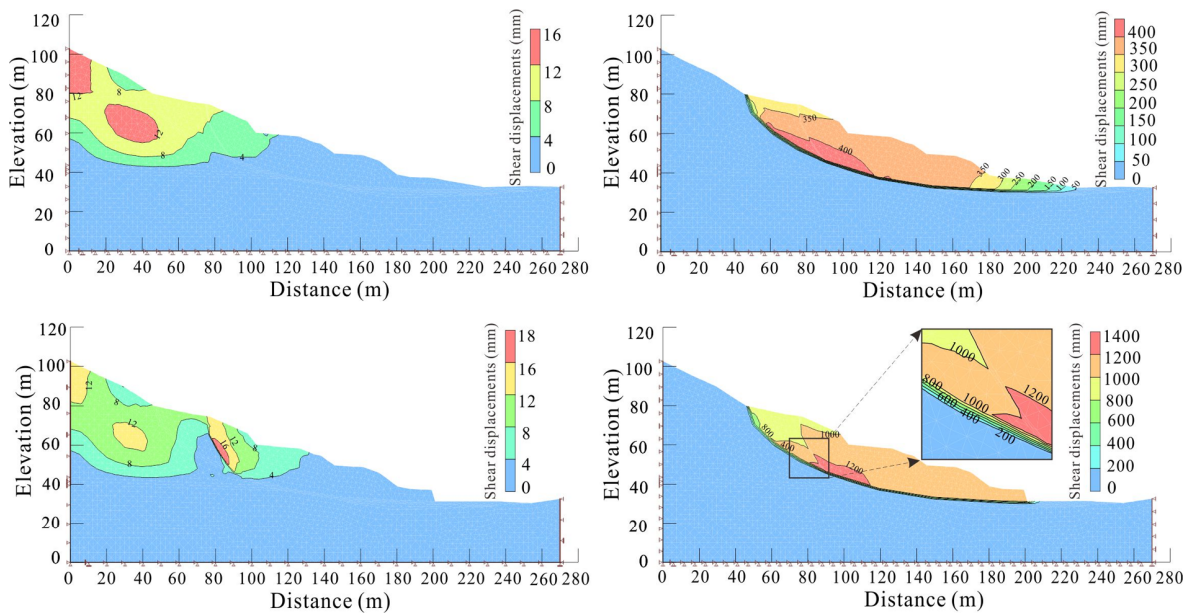


**Fig. 11** The shear displacement contour map. (a) Natural slope; (b) Natural slope after heavy precipitation; (c) Natural slope after excavation; (d) Natural slope after excavation and precipitation.

the depth of the trailing edge of the slope, with the magnitude of about 32 kPa. The maximum shear strain in this zone is very small, with only about 0.0008% (Fig. 10a). In addition, the maximum shear displacement of the slope is around 0.012 m (Fig. 11a), with the  $F_s$  about 1.424 (Table 4), indicating that the slope is under stable state. Upon the heavy precipitation infiltration, the stress, strain and displacement of soils changed dramatically compared with that of soils under the natural state (Figs. 9b-11 b). To be more specific, the peak value of shear stress

of soils after applying heavy precipitation increases to 60 kPa, and the location of the maximum shear stress moves to the front of the slope (Fig. 9b). Furthermore, the maximum shear strain that distributed in strips inside the slope is about 0.12% shown in Fig. 10b. The area zone with large deformation is further increased in the middle of the slope, and the maximum displacement is found to be 0.4 m (Fig. 11b). At this time, the factor of safety decreases to 1.032 (Table 4), illustrating that the soils are in an under-stable state (pre-sliding state).

### 5.3 Stress, deformation and failure caused by excavation

The excavation is simulated by setting the weight to be zero for the elements near the toe of the slope. With the excavation, the displacement and the stress at the toe of the slope is adjusted and gradually redistributed.

Figs. 9c-11c show the shear stress contour map, the shear strain contour map and the shear displacements contour map after the toe of the slope was excavated. The maximum shear stress is distributed deep in the middle of the slope, with the magnitude of about 32 kPa (Fig. 9c). The maximum shear strain was found to be about 0.016% (Fig. 10c). The displacements of soils after excavation have a small magnitude (with the maximum deformation only about 0.016 m), and it is observed that the excavation only affect a small area of the slope that is near the excavation zone (Fig. 11c). The computed  $F_s$  with respected to excavation is roughly 1.311 (Table 4), implying that the slope is under a stable state. With the calculated results, it can be concluded that no failure process occurs in the slope induced by the excavation activities at the toe of the slope. However, it should be noted that the excavation activities caused the decrease of factor of safety (from 1.424 to 1.311).

### 5.4 Stress, deformation and failure caused by excavation and precipitation

Under the combined effect of excavation and heavy precipitation, the stress and deformation of soils changes greatly compared with that of soils under natural state. For instance, the distribution zone of the shear stress expanded, and the maximum shear stress jumped to about 63 kPa (Fig. 9d). The shear strain is distributed in strips and has a wide range of distribution, with the maximum shear strain of 0.375% (Fig. 10d). The distribution of shear displacement zone increased, with the maximum value of shear displacement of 1.2 m (Fig. 11d). At this time, the  $F_s$  of the slope is 0.876 (Table 4), which means that the slope is in unstable state.

Compared with excavation activities, precipitation has a more influence on the stress, deformation and factor of safety of loess-mudstone slopes (Figs. 9-11). Therefore, a slope failure is prone to occurring by applying precipitation after the slope was excavated.

## 6 Formation Mechanism

### 6.1 Factors triggering loess-mudstone landslides

The occurrence of a landslide is controlled by internal factors such as geological structure, lithology, mineral composition, groundwater, topography and landform (Huang et al. 2017; Lian et al. 2020; Mu et al. 2019). Generally, the factors influencing the landslide occurrences can be mainly divided into two types: one is natural factors mainly including precipitation, flood, fluctuation of groundwater level, earthquake, etc., the other is artificial factors such as mining, slope excavation and loading on the top of a slope (Bhasin et al. 2002; Dai et al. 2001; Peng et al. 2015; Wang et al. 2019). Taking the DJG landslide as an example, the factors of triggering loess-mudstone landslides are analyzed in the perspective view of lithology, precipitation and artificial activities that caused the stress redistribution in the slope according to the field investigation, numerical simulation and the monitoring data obtained from literature.

#### 6.1.1 Lithology

The slip zone soils of loess-mudstone landslides are a mixture of loess soils, strong weathered Tertiary mudstone and bed rocks (Fig. 1c-d) in Yan'an area of China, among which the loess soils and mudstone are the materials basis in the formation of loess-mudstone landslides. Due to the unique characteristics of loess soils such as collapsibility, loose structure, well-developed pores and vertical joints with fractures (Fig. 12a-c), the surface water infiltrate downward easily. Furthermore, the strong

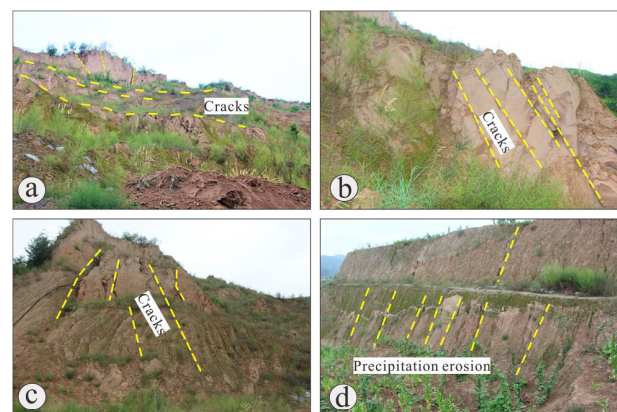


**Fig. 12** Field investigation. (a) Cracks at the back part of the landslide; (b) Cracks in the sliding debris; (c) Cracks in the side wall of the landslide; (d) The excavated steps exposed to the precipitation erosion.

weathered Tertiary mudstone which are featured by a dense structure, a low permeability and a small thickness, will develop into a water-resisting layer above the underlying bed rocks. In addition, the strong weathered Tertiary mudstone has been characterized by a low plastic limit and a low liquid limit, which facilitates the development of a weakening zone (Fig. 1d) owing to a sharp reduction in the shear strength upon water infiltration. The subsequent formation of a slip surface shown in Fig. 1f is associated with the formation of a weakening layer, which causes a reduction in the slope stability and eventually results in the slope failure.

### 6.1.2 Precipitation

Yan'an is characterized by a plateau continental monsoon climate, with cold, dry winters and hot, somewhat humid summers (Hou et al. 2000), in which the annual precipitation is only about 507.7 mm in the area (Han et al. 2018). However, most precipitation are rainstorms and heavy precipitation, and mainly concentrated in the summer months (June, July and August) and the autumn months (September and October) as shown in Fig. 2. Specially, the extreme precipitation events concentrate mainly in July and August in accompany with the frequent occurrence of landslides, which may be explained as follows: on the one hand, the self-weight of soils increases due to the precipitation infiltration and the sliding force increases subsequently. This process is continued until the sliding force exceeds the shear resistance, leading to the slope instability. On the other hand, precipitation infiltrates deep into the soil through seepage channels such as cracks and well-developed large pores (Fig. 12c). Consequently, the water content of the soils at lower layers increases and the saturated zone area expands as well. In addition, the water isolation effect of palaeo-soil or bedrock causes the formation of the upper perched water zone on the contact surface and the underground water level to rise, which leads to the softening of soils, the decrease of effective stress and a rapid reduction in shear strength, and thus the subsequent occurrence of landslides.

### 6.1.3 Artificial activities

Artificial activities such as irrigation and excavation have been identified as the main factors triggering landslides (Bui et al. 2016; Peng et al. 2019). For instance, under unloading effect caused by the excavation constructions on the original old landslide

(Fig. 12d), some evident extension cracks were found at the slope of the old landslide. In addition, the excavation activities for foundation construction at the toe of the slope in recent years (Fig. 1d) has caused the shear resistance of the sliding mass to dramatically decrease, and resulted in the redistribution of the stress within slope. Consequently, the stress concentration occurred at the toe of the slope and thus caused the creep phenomenon.

As mentioned above, the unique lithology in the study area is the material basis for the landslides occurrence and the seasonal precipitation is the main factor triggering the landslides. Moreover, the frequent excavation activities for the foundation construction at the toe of the slope are also a fundamental cause triggering landslides. In actual engineering, a progressive failure would occur due to the reduction in the shear resistance owing to the effect of the multiple factors mentioned above.

## 6.2 Formation mechanism of loess-mudstone landslides

The formation and evolution process of loess-mudstone landslides are controlled by the water sensitivity, permeability heterogeneity, topographic features and unique characteristics of slip zones soils (Kimura et al. 2015; Li et al. 2016; Wen et al. 2005). Taking the DJG landslide as an example, the formation mechanism of loess-mudstone landslides was illustrated in the following stages, namely, the local deformation stage, the penetration stage and the creeping-sliding stage.

(i) The local deformation stage: due to the change in the slope shape or the excavation at the toe of a slope, the stress state of the slope changes, and thus the creep movement toward empty face of the slope occurs. Due to the strong collapsibility of loess, the creeping phenomenon develops continually in the slope, the vertical joints in the middle and back part of the slope are thus pulled apart, which are displayed in the forms of the tensile cracks at the back edge of the slope on a macroscopic scale (Fig. 13a-b).

(ii) The penetration stage: Under the combined effect of the self-weight of the slope and precipitation, the creep deformation keeps continuing to accumulate and develops from the surface to the inside of the slope, causing the soils at the lower layers to be compressed and the shear stress increases in the slope. As the contact zone soils of loess-mudstone landslides are the

weakening layer that has the lowest shear resistance, therefore, a sliding surface gradually develops and penetrates along the contact zone soils, forming a complete sliding surface (Fig. 13c-d).

(iii) Creeping-sliding stage: With the further development of the sliding surface, the creep deformation of the slope accumulates as well. Thus, the energy accumulated during the creep process of the slope body is suddenly released, and the slope body slides down quickly and suddenly, resulting in a landslide hazard (Fig. 13d).

### 6.3 Limitations and future research

To calculate the shear behavior of soils in slope, the Mohr-Coulomb model which is simple and easily determinable model parameters in engineering applications was adopted in current study. However, the Mohr-Coulomb model which is a linear elastic-perfectly plastic model, may not be the first choice for simulating the slip zone soils which exhibits strain-softening behavior in current study. Thus, proposing a constitutive model which can describe the strain-softening behavior of slip zone soils and creating the

coupled model into the software are needed in our future research. Additionally, the stability of slope with different moisture contents was not discussed as well due to the fact that the infiltration process of water into the slope is a spatio-temporal evolution, which makes it difficult to determine the area and the distribution of slip zone soils affected, the time required for soils to achieve the specific saturated degree. Therefore, developing a conceptual modeling which can simulate water infiltrate into soils such as slip zone soils, Q<sub>3</sub> loess, Q<sub>4</sub> loess and mudstone with dynamically wettability would be our future investigation.

### 7 Conclusions

The instability of a loess-mudstone slope, which was induced by the excavation, was investigated. Based on the ring shear tests, the field investigation and the associated numerical simulation, the formation mechanism of loess-mudstone landslides induced by excavation and precipitation conditions was analyzed. The following conclusions can be drawn:

(1) The experimental results showed that the peak strength and residual strength of slip zone soils

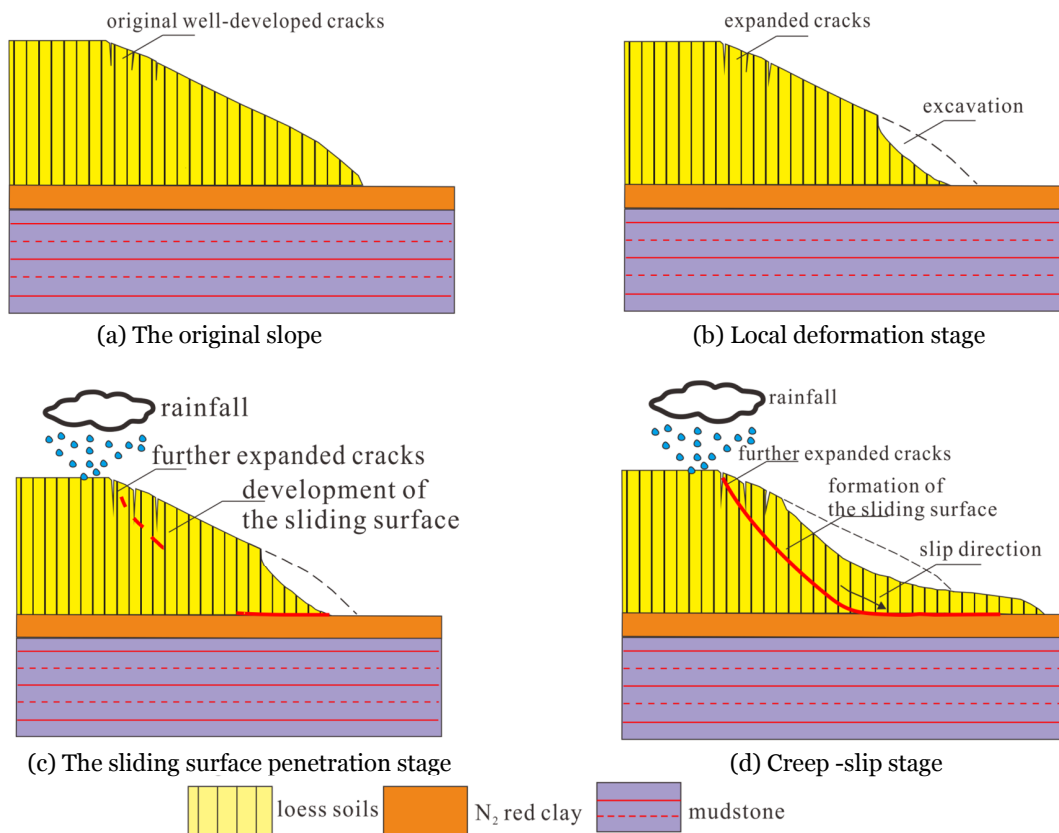


**Fig. 13** Formation mechanism of loess-mudstone landslides in the study area.

of loess-mudstone landslides decreased with moisture content, while the decrease of normal stress of slip zone soils caused the reduction in the shear strength, indicating that the rise in moisture content induced by precipitation and the drop in the normal stress would result in the weakening of shear strength of slip zone soils and triggering the landslides hazards eventually.

(2) A numerical model was established to simulate the excavation and precipitation infiltration process on the slope. According to the numerical simulation results, heavy precipitation changed the stress, strain and displacement distribution in the slope and caused the factor of safety of the slope to decrease, leading to the slope in the pre-sliding state, whereas the excavation only affected the stress balance of soils in slope that is near the excavation zone. The combined effect of excavation and heavy precipitation caused the factor of safety to decrease greatly and triggered landslide hazards, while the heavy precipitation played a more important role compared with excavation.

(3) The field investigation and numerical simulation results illustrated that the loess-mudstone slope, which is mainly composed of loess soils and

strongly weathered Tertiary mudstone, could develop into a landslide due to the fact that the loess soils that have the unique characteristics such as collapsibility, loose structure, well-developed pores and vertical joints allow the surface water infiltrate downward easily and the strong weathered Tertiary mudstone that has been characterized by a low plastic limit and a low liquid limit facilitates the development of a weakening zone. Thus, the loess soils and mudstone together provide material basic for the formation of loess-mudstone landslides. It's also found that the seasonal precipitation is the main factor triggering the landslides.

(4) The deformation and failure process of the loess-mudstone landslides underwent three stages, namely, the local deformation stage, the penetration stage, the creeping-slide stage. The creep movement of soils toward the empty face of the slope occurs due to the excavation activities and the sliding surface develops and penetrates eventually in the weakening layer soils under the effect of heavy precipitation. Consequently, the energy accumulated during the creep process of the slope body was suddenly released, and the slope body slip down quickly and suddenly, resulting in a landslide hazard.

## Acknowledgments

The authors thank to the anonymous reviewers and editors for their thoughtful review comments and suggestions which have significantly improved this paper. This research was supported by the National Natural Science Foundation of China (No.41902268)

and the China Postdoctoral Science Foundation (No. 2019T120871). Thanks also go to anonymous reviewers whose comments and suggestions have helped greatly improve the manuscript.

## References

- ASTM (2006) Annual Book of ASTM Standards. ASTM International, West Conshohocken, PA.
- Bhasin R, Grimstad E, Larsen JO, et al. (2002) Landslide hazards and mitigation measures at Gangtok, Sikkim Himalaya. *Eng Geol* 64(4): 351-368. [https://doi.org/10.1016/S0013-7952\(01\)00096-5](https://doi.org/10.1016/S0013-7952(01)00096-5)
- Bui DT, Tuan TA, Klempe H, et al. (2016) Spatial prediction models for shallow landslide hazards: a comparative assessment of the efficacy of support vector machines, artificial neural networks, kernel logistic regression, and logistic model tree. *Landslides* 13(2): 361-378. <https://doi.org/10.1007/s10346-015-0557-6>
- Caendish JC, Field DA, Frey WH (1985) An approach to automatic three - dimensional finite element mesh generation. *Int J Numer Methods Eng* 21(2): 329-347. [https://doi.org/10.1016/0010-4485\(85\)90219-2](https://doi.org/10.1016/0010-4485(85)90219-2)
- Chen J, Dai F, Xu L, et al. (2014) Properties and microstructure of a natural slip zone in loose deposits of red beds, southwestern China. *Eng Geol* 183: 53-64. <https://doi.org/10.1016/j.enggeo.2014.10.004>
- Code for geological investigation of landslide prevention, GB/T32864-2016, 2006. China Standardization Press, Beijing.
- Cremonesi M, Frangi A, Perego, U(2011) A Lagrangian finite element approach for the simulation of water-waves induced by landslides. *Comput Struct* 89(11-12): 1086-1093. <https://doi.org/10.1016/j.compstruc.2010.12.005>
- Dai F, Lee C, Li J, et al. (2001) Assessment of landslide susceptibility on the natural terrain of Lantau Island, Hong Kong. *Environ Geol* 40(3): 381-391. <https://doi.org/10.1007/s002540000163>
- Ding H, Shu C, Yeo K, et al. (2007) Numerical simulation of flows around two circular cylinders by mesh - free least square - based finite difference methods. *Int J Numer Methods Fluids* 53(2): 305-332. <https://doi.org/10.1002/flid.1281>
- Eid HT, Rabie KH, Wijewickreme D (2016) Drained residual

- shear strength at effective normal stresses relevant to soil slope stability analyses. *Eng Geol* 204: 94-107.  
<https://doi.org/10.1016/j.enggeo.2016.02.003>
- Erzin Y, Cetin T (2013) The prediction of the critical factor of safety of homogeneous finite slopes using neural networks and multiple regressions. *Comput Geosci* 51(51): 305-313.  
<https://doi.org/10.12989/gae.2014.6.1.001>
- Garga VK, Brown JD, Andresen A, et al. (1971) A New Ring Shear Apparatus and Its Application to the Measurement of Residual Strength. *Geotechnique* 21(4): 273-328.  
<https://doi.org/10.1680/geot.1971.21.4.273>
- Gibo S, Egashira K, Ohtsubo M (1987) Residual strength of smectite-dominated soils from the Kamenose landslide in Japan. *Can Geotech J* 24(3): 456-462.  
[https://doi.org/10.1016/0148-9062\(88\)91526-4](https://doi.org/10.1016/0148-9062(88)91526-4)
- Gibo S, Egashira K, Ohtsubo M, et al. (2002) Strength recovery from residual state in reactivated landslides. *Geotechnique* 52(9): 683-686.  
<https://doi.org/10.1680/geot.2002.52.9.683>
- Han L, Zhu H, Zhao Y, et al. (2018) Analysis of variation in river sediment characteristics and influential factors in Yan'an City, China. *Environ Earth Sci* 77(13): 479.  
<https://doi.org/10.1007/s12665-018-7664-3>
- Hou Q, Han R, Li H (2000) On the Problem of Vegetation Reconstruction in the Yan'an Experimental Area I. Conditions of Soil Water and Division of Vegetation Reconstruction. *Research of Soil & Water Conservation* 7(2): 103-110. (In Chinese)
- Huang R, Chen G, Tang P (2017) Precursor information of locking segment landslides based on transient characteristics. *Chin J Rock Mech Eng* 36(3): 521-533.  
<https://doi.org/10.13722/j.cnki.jrme.2016.1100>
- Juang CH, Dijkstra T, Wasowski J, et al. (2019) Loess geohazards research in China: Advances and challenges for mega engineering projects. *Eng Geol* 251: 1-10.  
<https://doi.org/10.1016/j.enggeo.2019.01.019>
- Kimura S, Nakamura S, Vithana SB (2015) Influence of effective normal stress in the measurement of fully softened strength in different origin landslide soils. *Soil Tillage Res* 145: 47-54.  
<https://doi.org/10.1016/j.still.2014.07.018>
- Li C, Yao D, Wang Z, et al. (2016) Model test on rainfall-induced loess-mudstone interfacial landslides in Qingshuihe, China. *Environ Earth Sci* 75(9): 1-18.  
<https://doi.org/10.1007/s12665-016-5658-6>
- Lian B, Peng J, Wang X, et al. (2019) Moisture content effect on the ring shear characteristics of slip zone loess at high shearing rates. *Bull Eng Geol Environ* 79(2): 999-1008.  
<https://doi.org/10.1007/s10064-019-01597-w>
- Lian B, Peng J, Zhan H, et al. (2020) Formation mechanism analysis of irrigation-induced retrogressive loess landslides. *Catena* 195(9): 104441.  
<https://doi.org/10.1016/j.catena.2019.104441>
- Maksimovic M (1989) Nonlinear failure envelope for soils. *J Geotech Eng* 115(4): 581-586.  
[https://doi.org/10.1061/\(asce\)0733-9410\(1989\)115:4\(581\)](https://doi.org/10.1061/(asce)0733-9410(1989)115:4(581))
- Motoyuki, Suzuki, Takeo, et al. (2000) Residual strength of soil by direct shear test. *Proceedings of JSCE* 645: 37-50.  
[https://doi.org/10.2208/jscej.2000.645\\_37](https://doi.org/10.2208/jscej.2000.645_37)
- Mu W, Wu X, Qian C, et al. (2019) Triggering mechanism and reactivation probability of loess-mudstone landslides induced by rainfall infiltration: a case study in Qinghai Province, Northwestern China. *Environ Earth Sci* 79(1): 22.  
<https://doi.org/10.1007/s12665-019-8767-1>
- Mulligan R, Franci A, Celiueta M, et al. (2020) Simulations of landslide wave generation and propagation using the Particle Finite Element Method. *J Geophys Res: Oceans* 125(6).  
<https://doi.org/10.1029/2019jco15873>
- Peng J, Fan Z, Wu D, et al. (2019) Landslides triggered by excavation in the loess plateau of China: A case study of Middle Pleistocene loess slopes. *J Asian Earth Sci* 171: 246-258.  
<https://doi.org/10.1016/j.jseaes.2018.11.014>
- Peng J, Fan Z, Wu D, et al. (2015) Heavy rainfall triggered loess-mudstone landslide and subsequent debris flow in Tianshui, China. *Eng Geol* 186: 79-90.  
<https://doi.org/10.1016/j.enggeo.2014.08.015>
- Peng J, Leng Y, Zhu X, et al. (2016) Development of a loess-mudstone landslide in a fault fracture zone. *Environ Earth Sci* 75(8): 658.  
<https://doi.org/10.1007/s12665-016-5336-8>
- Sassa K, Fukuoka H, Wang G, et al. (2004) Undrained dynamic-loading ring-shear apparatus and its application to landslide dynamics. *Landslides* 1(1): 7-19.  
<https://doi.org/10.1007/s10346-003-0004-y>
- Tiwari B, Marui H (2005) A new method for the correlation of residual shear strength of the soil with mineralogical composition. *J Geotech Geoenviron Eng* 131(9): 1139-1150.  
[https://doi.org/10.1061/\(asce\)1090-0241\(2005\)131:9\(1139\)](https://doi.org/10.1061/(asce)1090-0241(2005)131:9(1139))
- Vithana SB, Nakamura S, Gibo S, et al. (2012) Correlation of large displacement drained shear strength of landslide soils measured by direct shear and ring shear devices. *Landslides* 9(3): 305-314.  
<https://doi.org/10.1007/s10346-011-0301-9>
- Wang G, Zhang D, Furuya G, et al. (2014) Pore-pressure generation and fluidization in a loess landslide triggered by the 1920 Haiyuan earthquake, China: A case study. *Eng Geol* 174 (1): 36-45.  
<https://doi.org/10.1016/j.enggeo.2014.03.006>
- Wang W (2014) Residual Strength of Remolded Loess in Ring Shear Tests. PhD thesis, Northwest A & F University of China, Shaanxi, China. pp 35-37. (In Chinese)
- Wang X, Wang J, Zhan H, et al. (2019) Moisture content effect on the creep behavior of loess for the catastrophic Baqiao landslide. *Catena* 187: 104371.  
<https://doi.org/10.1016/j.catena.2019.104371>
- Wen B, Aydin A (2003) Microstructural study of a natural slip zone: quantification and deformation history. *Eng Geol* 68(3-4): 289-317.  
[https://doi.org/10.1016/s0013-7952\(02\)00234-x](https://doi.org/10.1016/s0013-7952(02)00234-x)
- Wen B, Wang S, Wang E, et al. (2005) Deformation characteristics of loess landslide along the contact between loess and neocene red mudstone. *Acta Geol Sin-Engl Ed* 79(001): 139-151.  
<https://doi.org/10.1111/j.1755-6724.2005.tb00875.x>
- Wen BP, He L (2012) Influence of lixiviation by irrigation water on residual shear strength of weathered red mudstone in Northwest China: Implication for its role in landslides' reactivation. *Eng Geol* 151: 56-63.  
<https://doi.org/10.1016/j.enggeo.2012.08.005>
- Wu W, Su X, Liu W, et al. (2014a) Loess-mudstone interface landslides: characteristics and causes. *J Glaciol Geocryol* 36(5): 1167-1175.  
<https://doi.org/10.7522/j.issn.1000-0240.2014.0139>
- Xu C, Wang X, Lu X, et al. (2018) Experimental study of residual strength and the index of shear strength characteristics of clay soil. *Eng Geol* 233(3): 183-190.  
<https://doi.org/10.1016/j.enggeo.2017.12.004>
- Yuan W, Fan W, Jiang C, et al. (2019) Experimental study on the shear behavior of loess and paleosol based on ring shear tests. *Eng Geol* 250: 11-20.  
<https://doi.org/10.1016/j.enggeo.2019.01.007>
- Zhang Z, Wang T, Wu S, et al. (2017) Seismic performance of loess-mudstone slope in Tianshui-Centrifuge model tests and numerical analysis. *Eng Geol* 222: 225-235.  
<https://doi.org/10.1016/j.enggeo.2017.04.006>
- Zhao L, Cheng X, Dan H, et al. (2017) Effect of the vertical earthquake component on permanent seismic displacement of soil slopes based on the nonlinear Mohr-Coulomb failure criterion. *Soils Found* 57(2): 237-251.  
<https://doi.org/10.1016/j.sandf.2016.12.002>
- Zhu H, Randolph MF (2010) Large deformation finite-element analysis of submarine landslide interaction with embedded pipelines. *International Journal of Geomechanics* 10 (4): 145-152.  
[https://doi.org/10.1061/\(asce\)gm.1943-5622.0000054](https://doi.org/10.1061/(asce)gm.1943-5622.0000054)